



# Impact performance of hybrid laminated composites with statistical analysis

Marwa A. Abd El-baky<sup>1</sup>

Received: 30 October 2017 / Accepted: 10 April 2018 / Published online: 15 May 2018  
© Iran Polymer and Petrochemical Institute 2018

## Abstract

The main emphasis of this work is to fabricate a new composite system having high impact performance, light weight, cost-effective and reduced water absorption. Glass (G)–polypropylene (P) fibers reinforced epoxy composite laminates were fabricated using the hand lay-up technique. The impact response and water absorption capabilities of G–P fibers reinforced epoxy composites were investigated to know their suitability and adaptability for different industrial applications. Morphological studies of the fractured surfaces were performed using scanning electron microscopy (SEM). Two-parameter Weibull distribution function was used to obtain the scatter in the results and to construct the reliability graphs. These reliability graphs are important tools for helping the designers to understand and choose the suitable material for the required application. The proposed G–P/epoxy hybrid composites showed an improvement in the impact performance and reduction in water absorption capability compared to the host composites. The hybrid composite with G-fiber at the periphery and P-fiber at the core has lower void content and lower water uptake. The plies stacking sequence has almost no effect on edge-wise impact strength values, whilst it has a noticeable effect on flat-wise impact strength values. When P-layers are at the impacted face, the composite exhibits higher impact strength. Both edge-wise and flat-wise impact strengths increase when P/G fiber ratio increases.

**Keyword** Hybrid composites · Polypropylene and glass fibers · Impact resistance · Voids · Water absorption

## Introduction

Composites have found numerous applications in aerospace, automotive, and construction industries owing to their light weight, high specific strength, high specific stiffness, and other performance benefits [1]. Composite structures are prone to impact loadings during service life, which significantly can cause inner damages, such as matrix cracking, interfacial debonding and delamination [2]. Impact behavior of composite materials is controlled by many factors such as the nature of the matrix, the nature, content, length and orientation of the reinforcement, the fiber–matrix interface and hybrid design [3, 4]. To improve the impact energy-absorbing ability of composites, high strain-to-failure fibers can be added to the host composite, realizing hybrid composites [5].

Hybrid composites are materials fabricated by incorporating two or more different reinforcements in a common matrix to obtain a synergistic improvement in the mechanical and physical properties. The hybrid reinforcements achieve a performance that cannot be obtained using a single reinforcement type. Hybrid composite approach aims to reduce the production cost by the proper selection of reinforcing materials. A compromise between the performance and cost could be achieved [6]. Hybridization process has proved to be an effective method to design materials suited for various requirements [7].

Various studies have been reported on the impact performance of hybrid composites. Pothan et al. [8, 9] studied the impact properties of banana-glass/polyester hybrid composites with different layering patterns. It was concluded that the composite with five layers, where glass forms both the core and the skin is giving the highest impact properties. Pincheira et al. [10] evaluated the influence of the reinforcing aramid fibers in carbon/epoxy composites. The presence of aramid phase in the hybrid carbon/aramid composite induced a significant enhancement in the impact (37.9% in

✉ Marwa A. Abd El-baky  
dr.marwa2013@yahoo.com

<sup>1</sup> Mechanical Design and Production Engineering Department,  
Zagazig University, Zagazig 44519, Egypt

energy absorption) and fracture resistance (12.7% for fracture initiation and 43% for steady state regime). Davoodi et al. [11] noticed that the impact strength of kenaf–glass/epoxy hybrid composites is lower than that of common glass/epoxy one. Boopalan et al. [12] found that the addition of banana fiber to jute/epoxy composites gives 35.5% increase in the impact strength. Dehkordi et al. [13] examined the impact behavior of hybrid composites based on basalt and nylon woven fabrics. The results indicated that impact performance of these composites is significantly affected by the nylon/basalt fiber content. Wang [14] evaluated the impact performances of interply and intraply basalt–kevlar/epoxy hybrid composites. The results showed that the interply hybrid composite has higher ductile indices, lower peak load, and higher specific energy absorption in both warp and weft directions compared to intraply hybrid. Panthapulakkal et al. [15] enhanced the impact properties of hemp/polypropylene composite by hybridizing it with small amounts of glass fiber. Venkateshwaran et al. [16] showed that the addition of sisal fiber to banana/epoxy composites by 50% by weight results in 35% increase in the impact strength.

Polymer composites are often used in applications where exposed to water such as marine applications, fishing trawlers, canoes, patrol boats and submarine domes [17]. All polymer composites absorb moisture under humid atmosphere and by immersion in water. The effect of absorption of moisture leads to the degradation in fiber–matrix interface region creating poor stress transfer efficiency resulting in a reduction in mechanical and dimensional properties [18]. To achieve the full potential of polymer composites, they must have good environmental stability. The major factors that control the interaction between fibers and water are diffusion, permeability, and sorption. The swelling behavior of the fibers is greatly affected by its physical and chemical structures [19]. Various studies have been reported on the phenomenon of moisture absorption in polymer hybrid composites.

Koradiya et al. [20] noticed an improvement in water absorption behavior of jute–glass/epoxy composites compared to pure jute composite. Water uptake of silk–glass hybrid composites was found to be less than that of unhybridized silk reinforced composite [21]. Panthapulakkal et al. [15] deduced that the incorporation of glass fiber into hemp/polypropylene composites improves their water resistance. Jarukumjorn et al. [22] enhanced water resistance of sisal/polypropylene composites by adding glass fiber. Joseph et al. [23] found that water uptake of banana reinforced composite decreases with the incorporation of glass fiber. The composites with glass fiber at the periphery and banana fiber at the core have maximum resistance to water absorption.

Mechanical properties of polymer composite exhibit wide variability even with specimens prepared and tested under identical conditions. This is due to several factors such as the

specimen manufacturing, preparation, handling, storage, test rig design, and experimental technique. However, the most important source of variability associated with the material nature has received little attention [24]. Weibull distribution function has proved to be a useful and versatile method for describing the properties of composite structures. This is because the probability density function (PDF) of Weibull distribution has a wide variety of shapes. Weibull cumulative distribution function (CDF) is equivalent to the normal distribution with the shape parameter of  $\alpha = 3.2$ . Rayleigh distribution is Weibull distribution with  $\alpha = 2.0$  [25]. The scatter in the mechanical properties for composites is usually described by, two or three-parameter Weibull distribution [26]. Two-parameter Weibull distribution was previously used by Mottram [27] to examine the compressive strength data of flat pultruded panels. Also, Selmy et al. [28] used it to analyze the tensile, flexural, in-plane, and interlaminar shear properties of unidirectional glass fiber-random glass fiber/epoxy hybrid composites. The most popular techniques used to calculate the shape and scale parameters ( $\alpha$ ) and ( $\beta$ ) of Weibull function are the graphical method and the maximum-likelihood method [29].

Lightweight materials are becoming important in many industries, such as automotive, aviation, marine, wind energy, portable electronics, and so on. P-fiber is characterized by its low density, low cost and high ductility, whereas G-fiber is commercially used for its high strength, high stiffness, low water absorption and availability. The lack of data on G–P hybrid composites is the rationale behind this experimental work, whose aim is to provide a comprehensive investigation on the impact behavior and water absorption of G–P-fibers reinforced hybrid composites. To approach this aim, unidirectional G–P/epoxy hybrid composites were fabricated in intraply and inter-intraply hybrid structures using the hand lay-up technique. The fabricated composites were subjected to impact loading in edge-wise and flat-wise directions. Specimens with different lay-ups and different P/G fiber ratios were tested. The water absorption of the fabricated composites was evaluated by gravimetric analysis, i.e. by the measurement of the relative weight uptake of the aged specimens in accordance with the exposure time. The results were used to understand the role played by the hybridization process between G-fiber and P-fiber on the impact behavior and water absorption characteristics.

## Experimental work

### Materials

The materials which were used to make the proposed hybrid composites included unidirectional G-fiber (2400 g/km) and unidirectional P-fiber (550 g/km) supplied by El-Kariem

(Egypt) and El-Nassagoun El-Sharquioun (Egypt), respectively. Kemapoxy 150 RGL, chosen as a matrix material, was supplied by Chemicals for Modern Building Group (Egypt).

### Preparation of the composites

A total of nine G–P fibers reinforced epoxy composite laminates were fabricated using the hand lay-up technique [30, 31]. The overall fiber volume fraction, i.e.  $V_f = V_{fP} + V_{fG}$ , and thickness of all the fabricated composites are approximately 32.5% and 7.25 mm, respectively. First, G and P-fiber bundles were fixed on wooden frames using small pins as shown in Fig. 1a. The distance between each adjacent two pins in the wooden frame was assigned as the pitch. The densities of G and P fibers were 2560 and 910 kg/m<sup>3</sup>, respectively. The G and P-fiber volume fractions in the fabricated composites were controlled by changing the pitch value as

shown in Table 1. Arranging the fiber bundles with this method ensured regular distribution of the fibers and kept them in place. The details of the fabricated composite laminates, their configuration, plies stacking sequence and fibers' relative volume fractions are listed in Table 1. The fabrication process of G–P fibers/epoxy composite laminates can be summarized as follows:

The lay-up mold was treated by a release agent and was left to dry. A layer of epoxy resin was spread on the mold. The first template with fiber bundles was placed on the resin. Next, they were rolled to distribute the matrix and displace the air outwards as shown in Fig. 1b. When the fibers were fully impregnated with epoxy, they were loosened from the template, and more epoxy was added and distributed. The procedure was repeated with alternate layers of matrix and fibers until the whole laminate was primarily constructed. When the last fiber layer was impregnated, a steel plate with

**Fig. 1** **a** Wooden templates with G-fiber bundles and P-fiber bundles, **b** rolling process, **c** a 25-kg steel plate placed on top of the laminate, and **d** final composite laminate

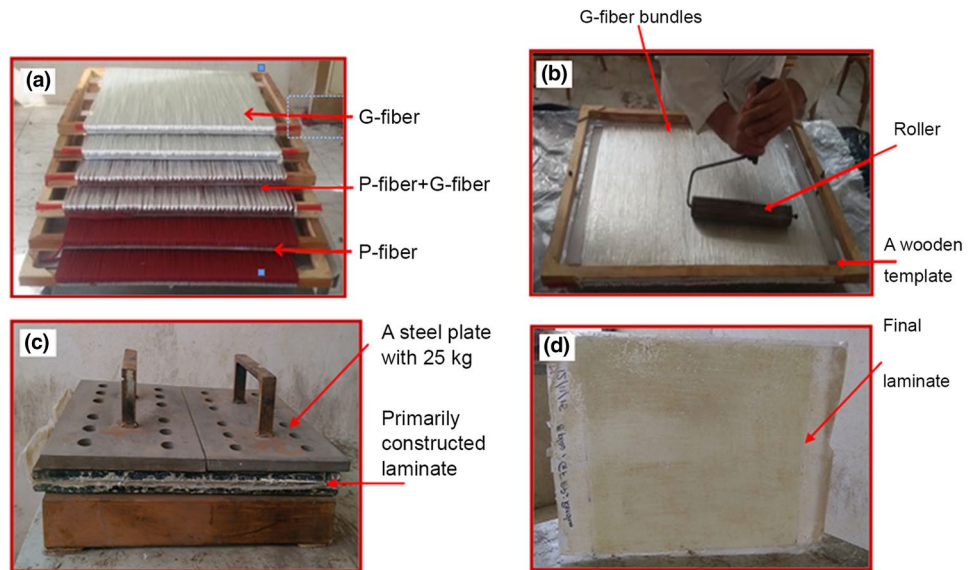


**Table 1** The details of the fabricated G–P fibers reinforced epoxy hybrid composites

Composite laminate code	Composite laminate type	Stacking sequence	Overall fiber volume fraction, $V_f$ (%)	Fibers relative volume fraction (%)		Pitch value on the wooden template (mm)	
				$V_{fG}$	$V_{fP}$	G-fiber	P-fiber
PFRP	Non-hybrid	[P] <sub>6</sub>	32.5	0.0	32.5	–	3
H1	Inter-intraply hybrid	[P <sub>2</sub> /GP <sub>2</sub> /G <sub>2</sub> ]	16.25	16.25	16.25	10	6
H2		[G <sub>2</sub> /GP <sub>2</sub> /P <sub>2</sub> ]				10	6
H3		[P/GP/G] <sub>s</sub>				10	6
H4		[G/GP/P] <sub>s</sub>				10	6
H5	Intraply hybrid	[GP] <sub>6</sub>	10.83	21.67	15	4.5	
H6		[GP] <sub>6</sub>	16.25	16.25	10	6	
H7		[GP] <sub>6</sub>	21.67	10.83	7.5	9	
GFRP	Non-hybrid	[G] <sub>6</sub>	32.5	0.0	5	–	

25 kg mass was placed on top of the laminate to obtain a uniform pressure and consequently a constant thickness for the fabricated composite as shown in Fig. 1c. Finally, the constructed laminate was left at room temperature until it was completely cured (Fig. 1d). The test specimens were prepared according to the corresponding standards.

### Density measurements

One important criterion for composite design is the weight which can be alternatively characterized by the density. The samples weights in air ( $P_d$ ) were measured by an electronic balance, with sensibility of  $\pm 0.0001$  g. The experimental density,  $\rho_{\text{exp}}$ , was calculated as follows:

$$\rho_{\text{exp}} = \rho_0 \left( \frac{P_d}{P_d - P_{\text{im}}} \right), \quad (1)$$

where  $\rho_0$ , the water density and  $P_{\text{im}}$  as the sample weight in water.

### Water absorption test

Water absorption capability of the fabricated composites has been studied at room temperature by the measurement of the relative weight uptake of the aged specimens in accordance with the exposure time as per ASTM D 570 [32]. Specimens were cut into  $50 \times 50$  mm<sup>2</sup>. They were weighed and then immersed in distilled and sea water up to the saturation point [33]. The percentage weight change was determined until the equilibrium values were reached. Specimens were removed from water at different times, wiped with tissue paper to remove surface water and weighed with electronic balance, with sensibility of  $\pm 0.0001$  g [34, 35]. In this study, no water gain was observed after 11 months. The water absorption study has given valuable information on the nature of the interface between G and P fibers and the matrix. The water absorption characteristics of G–P/epoxy specimens were evaluated by the relative uptake of weight defined by  $M_t$  according to the following equation [36]:

$$\text{Water absorption } (M_t) = \frac{P_w - P_d}{P_d}, \quad (2)$$

where  $P_w$  and  $P_d$  are the wet and dry weights of the sample, respectively.

### Izod impact tests

Impact behavior is a measure of the energy required to initiate the damage and progress the failure within the composite [37]. Impact strengths for the fabricated composites were measured using Izod impact testing machine (type Avery Denison) as per the ISO 180 [38]. The test specimens were

cut into  $64 \times 12.7$  mm<sup>2</sup>. Five identical specimens were tested in each case and the average value was reported. Two types of tests were performed; on one hand, un-notched coupons were impacted in the flat-wise direction, perpendicular to the layers; on the other hand, notched coupons were impacted in the edge-wise direction, parallel to the layers. For notched specimens, a 45° V-notch was inserted through the specimen thickness by milling process to a depth of 2.5 mm. The impact strength,  $S_n$  for notched edge-wise specimens and  $S_u$  for un-notched flat-wise specimens were calculated as follows:

$$S_n = \frac{\text{Absorbed energy}}{b_n h} \quad \text{and} \quad S_u = \frac{\text{Absorbed energy}}{b h}, \quad (3a,b)$$

where  $b$ ,  $b_n$  and  $h$  are respectively the specimen's width, residual width after inserting the notch and thickness.

Izod impact test procedure can be summarized as follows:

At first, the specimen was positioned in the vice with a centering device adapted as a vertical cantilever beam. It was secured by turning a hand wheel clockwise. A screw was made available just in the middle of the hand wheel to control the clamping torque applied by means of a dynamometric key with a resolution of 0.5 N m and a working torque range from 1 to 25 N m. Then, the hummer was set in the raised position. The pointer was set on upper limit of the scale as zero point. Finally, the hummer was released with a velocity of 3.65 m/s. The absorbed energy was recorded on the machine scale [39].

### Morphological analysis

Impact behavior damage in polymer composites depends on many parameters such as the fiber type, orientation and volume fraction, matrix type, lay-up sequence and fiber–matrix bond. Furthermore, polymer composites have various damage modes such as micro-cracking, matrix deformation, fiber–matrix debonding, fiber breakage, fiber pull-out and delamination. These various damage modes may appear singly or together. Morphological analysis was carried out using SEM to examine the failure of the impacted specimens. Fractured specimens were coated with gold and kept in an ionizer. The images of the fractured specimens were taken by subjecting them to a voltage of 20 kV.

### Hybrid effect

The hybrid effect is defined as the fractional deviation of the experimental property, i.e.  $P_{\text{exp}}$  compared to that estimated from the rule of mixtures (RoM), i.e.  $P_{\text{RoM}}$  and  $P_{\text{exp}}$  can be thus given by Eq. 4 [40]:

$$e_h = \frac{P_{\text{exp}}}{P_{\text{RoM}}} - 1 \quad (4)$$

## Specific impact strength

Specific impact strength can be calculated as the experimental value divided by the composite density. The use of specific properties is an essential concept when comparing the capabilities of composites fabricated from different materials. This approach is reasonable in all engineering applications, aiming for weight reduction [40].

## Strength-to-cost ratio

Cost is an important criterion in the design of composite structures. It is influenced by a combination of design and fabricating parameters. The key cost drivers for design are material selection, configuration and complexity. While those for manufacturing are related to labor and equipment costs and production volume. Approximately, 40% of the composite cost is due to material cost [41]. The material cost may be used as a reasonable proxy for the cost index. The material cost for a composite is the summation of its constituent costs. In this study, the costs of G-fiber, P-fiber and epoxy matrix are 2.5, 1.0 and 8 \$/kg.

## Theoretical work

### Fiber volume fraction ( $V_f$ )

The overall fiber volume fraction ( $V_f$ ) of the fabricated composites was obtained theoretically as follows:

First, a specimen from the composite was considered and its volume was determined ( $V_C$ ). Then, the length of the fiber bundles in the specimen ( $L$ ) was calculated. Finally, the weight of the fiber in the piece ( $M_f$ ) and the fiber volume ( $v_f$ ) were estimated using Eqs. 5 and 6. The estimated fiber volume fraction ( $V_f$ ) was calculated using Eq. 7:

$$M_f = \rho_l L \quad (5)$$

$$v_f = \frac{M_f}{\rho_f} \quad (6)$$

$$V_f = \frac{v_f}{V_C}, \quad (7)$$

where  $\rho_l$  and  $\rho_f$  are the linear density and volumetric density of the fiber.

### Density and void content

Following the RoM, the theoretical densities ( $\rho_{th}$ ) of the fabricated composites can be expressed as follows [42]:

$$\rho_{th} = \rho_{fP} V_{fP} + \rho_{fG} V_{fG} + \rho_m (1 - [V_{fG} + V_{fP}]), \quad (8)$$

where  $V$  is the volume fraction, the subscripts “fG” and “fP” refer to G and P fibers, respectively.

The void content is one of the most important problems that may be encountered in fiber-reinforced composites. The voids are produced inadvertently in composites either in manufacturing stage or while in service. The most common cause of voids is the incapability of the matrix to displace all the air entrapped within the fibers as it passes through the matrix. The existence of voids in the composite significantly reduces its mechanical and physical properties. During the impregnation of the fibers with the matrix, i.e. during the fabrication process, the trapped air or other volatiles may exist in the composites [43]. The void content of the fabricated composites were calculated according to ASTM D2734 [44] using Eq. 9:

$$\text{Void content} = \frac{(\rho_{th} - \rho_{exp})}{\rho_{th}} \quad (9)$$

## Statistical analysis of impact test data

As composites are inhomogeneous some wide differences may be seen in static strength test results under the same conditions. Statistical evaluations are very important because of wide distributions of the test results in composite samples. When a great safety coefficient was used in the past, this distribution in the results was relatively unimportant. With the development of high-performance aircraft, the changeability of mechanical properties of composites has gained great importance [45, 46]. Analyzing the reliability of composite materials is an inevitable need because of brittle fracture in structures and the wide scatter of experimental data. Thus, for the safe application of composite materials in industry, their data as statistically must be understood well. The statistical properties used, generally depend on usual distribution in mean strength. But especially, Weibull distribution has more reliable values than other distributions in mechanical data evaluations from the point of variables strength parameters [47, 48]. Therefore, it has been confirmed in the literature that Weibull distribution is useful in the evaluation of mechanical data reliability in composite structures [49, 50].

Two-parameter Weibull distribution is being used to model extreme values such as the failure strength. The advantages of two-parameter Weibull distribution are as follows:

- It can be explained with a simple function and applied easily.
- It is used frequently in the evaluation of mechanical properties of composites.
- Its usage is easy having present graphics and simple calculation methods.

- It gives some physical rules concerning failure when the slope of Weibull probability plots taken into account. The PDF of two-parameter Weibull distribution has been indicated in Eq. 10, [51, 52].

$$f(n) = \left(\frac{\alpha}{\beta}\right) \left(\frac{n}{\beta}\right)^{\alpha-1} \exp\left[-\left(\frac{n}{\beta}\right)^\alpha\right] \quad \alpha \geq 0, \quad \beta \geq 0, \quad (10)$$

where  $n$  is the random variable value,  $\alpha$  and  $\beta$  are the shape and scale parameters. In this study, the random variable is the impact strength.

If PDF equation is integrated, the CDF in Eq. 11 will be obtained. Equation 12 is derived from Eq. 11. Equation 13 represents the probability of survival or reliability ( $R_n$ ) and the probability of failure ( $P_n$ ).

$$F(n) = 1 - \exp\left[-\left(\frac{n}{\beta}\right)^\alpha\right] \quad (11)$$

$$\exp\left[-\left(\frac{n}{\beta}\right)^\alpha\right] = 1 - F(n) \quad (12)$$

$$R_n = 1 - P_n, \quad (13)$$

where  $R_n$  is the probability of survival or reliability and  $P_n$  is the probability of failure.

If the natural logarithm of both sides of Eq. 12 is taken, the following equation will be obtained:

$$\ln\left[\ln\left(\frac{1}{1-F(n)}\right)\right] = \alpha \ln(n) - \alpha \ln(\beta). \quad (14)$$

Equation 14 is rearranged to be  $Y = \ln\left[\ln\left(\frac{1}{1-F(n)}\right)\right]$ ,  $X = \ln(n)$ ,  $m = \alpha$  and  $c = -\alpha \ln(\beta)$ . Hence, a linear regression model in the form of Eq. 15 will be obtained as follows:

$$Y = mX + c \quad (15)$$

$$\beta = e^{(-c/\alpha)}. \quad (16)$$

In Eq. 11, when  $n = \beta$ ,

$$F(n) = 1 - \exp[-(1)^\alpha]$$

$$F(n) = 1 - 0.368 = 0.632 = 63.2\%.$$

According to Eq. 16, ( $\beta$ ) is the impact strength at which 63.2% of the population is expected to fail. In this study, reliability plots have been constructed to guide the designers. Mean value (M), standard deviation (SD) and coefficient of variation (CV) of impact strength values were calculated from Eqs. 17–19 as follows:

$$M = \beta\Gamma\left(1 + \frac{1}{\alpha}\right) \quad (17)$$

$$SD = b\sqrt{\left[\Gamma\left(1 + \frac{2}{\alpha}\right) - \Gamma^2\left(1 + \frac{1}{\alpha}\right)\right]} \quad (18)$$

$$CV = \frac{SD}{MTTF} = \frac{\sqrt{\left[\Gamma\left(1 + \frac{2}{\alpha}\right) - \Gamma^2\left(1 + \frac{1}{\alpha}\right)\right]}}{\Gamma\left(1 + \frac{1}{\alpha}\right)}, \quad (19)$$

where  $\Gamma$  is gamma function.

## Application of Weibull distribution

Weibull distribution parameters and the reliability analysis processes were carried out by Microsoft Excel. Steps to draw Weibull lines and obtain  $\alpha$  and  $\beta$  are shown as follows [48]:

1. The impact strength values are located and arranged in ascending order and a serial number was given for each value ( $i = 1, 2, 3, \dots, n$ ).
2. Each impact strength value is used in Bernard's Median Rank formula given in Eq. 20:

$$MR = \frac{i - 0.3}{n + 0.4} \quad (20)$$

where  $i$  is the failure serial number and  $n$  is total test number of samples.

3.  $\ln(\ln(1/(1 - MR)))$  and  $\ln(\text{impact strength})$  the values are calculated for each impact strength.
4. The graphics of  $\ln(\text{impact strength})$  and  $\ln(\ln(1/(1 - MR)))$  values are drawn.
5. Equation 15 is obtained in the most reasonable form from these graphics and  $\alpha$  and  $\beta$  values are calculated.
6. The mean impact strength and the coefficient of variation corresponding to each composite type are calculated using Eqs. 17 and 19.

## Results and discussion

### Fiber volume fraction

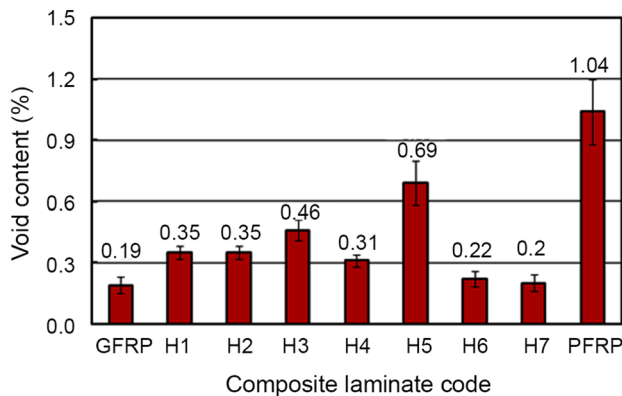
The overall fiber volume fraction and the relative fibers contents were calculated theoretically and listed in Table 1.

### Density and void content

As depicted in Table 2, there is a good agreement between the experimental and theoretical densities for all fabricated composites. The composite density decreases with

**Table 2** Specific impact strength and cost ratio for G–P fibers reinforced epoxy hybrid composites

Laminate code	Density (kg/m <sup>3</sup> )		Specific impact strength (J m/kg)		Cost ratio (10 <sup>4</sup> J/m <sup>2</sup> \$)	
	Theoretical, $\rho_{th}$	Experimental, $\rho_{exp}$	Edge-wise	Flat-wise	Edge-wise	Flat-wise
GFRP	1575	1571.58	105.33	83.43	1.08	0.86
H1	1306	1299.93	245.02	195.71	3.66	2.92
H2	1306	1299.93	245.02	166.46	3.66	2.48
H3	1306	1302.05	263.40	183.15	3.53	2.73
H4	1306	1301.34	234.69	167.08	3.50	2.49
H5	1199	1190.59	331.53	241.20	6.06	4.41
H6	1306	1303.04	236.75	171.59	3.93	2.56
H7	1414	1411.18	191.65	128.57	2.48	1.66
PFRP	1038	1026.98	466.57	348.55	22.23	16.61

**Fig. 2** Void content for the fabricated G–P fibers reinforced epoxy composites

increasing P-fiber content due to the lower density of P-fiber compared to G-fiber. The void content of the fabricated composites with different layering patterns is presented in Fig. 2. Pure P-fiber reinforced epoxy composite, PFRP, exhibits the highest void content (1.04%) compared to other composites. This may be due to the incompatibility between the epoxy resin and P-fiber. According to Abd El-baky et al. [50], incomplete wetting out of the fibers by the matrix leads to the formation of voids. On the other hand, the lowest void content (0.19%), is associated with pure G-fiber reinforced epoxy composite, GFRP. As expected, hybrid composites have intermediate void content between PFRP and GFRP composites.

For intraply hybrid composites, as P/G ratio increases, the void content increases, i.e. hybrid composite containing higher P-fiber amount, i.e. H5 has higher void content. For the studied inter-intraply hybrid composites, it was noticed that the plies stacking sequence has a significant effect on the void content. The composite with G-fiber at the skin and P-fiber at the core, i.e. H4 has lower void content (0.31%) compared with the hybrid with the opposite arrangement,

i.e. H3 (0.46%). That is because P-fiber in the specimen core is tightly packed by G-fiber. However, it is clear from Fig. 2 that the hand lay-up technique leads to a satisfactory fiber impregnation level and results in composites with low void contents. Void content less than 1% is required for aerospace applications and 5% is acceptable for other applications such as automotive and marine [50].

### Water absorption

Figure 3 shows water uptake of G–P fibers/epoxy composite specimens immersed in distilled and sea water. It is clear from Fig. 3 that the rate of diffusion of water into G–P fibers reinforced composites is time dependent. Composites absorb water very rapidly at the initial stage and later a saturation level could be attained without any further increase. Water uptake of PFRP composite is the highest whilst that of GFRP composite is the lowest. This is due to the hydrophilic nature of P-fiber and due to the capillary action when fiber ends are exposed to water [36]. Hybrid composites have intermediate water absorption capability between those of PFRP and GFRP composites. Water absorption of hybrid composites decreases by the incorporation of G-fiber due to the negligible water absorption capacity of water impermeable G-fiber, as compared with P-fiber. Hybrid composite with G-fiber at the periphery and P-fiber at the core, i.e. H4 may display maximum resistance toward water absorption because G-fiber acts as a barrier to P-fiber, thus preventing the direct contact between P-fiber and water. Whilst the hybrid with the opposite arrangement, i.e. H3, may display minimum resistance toward water absorption. As P-fiber amount increases, water absorption increases due to the presence of a high amount of P-fiber and a large number of porous tubular structures or voids. The presence of G-fiber makes the composite more hydrophobic in nature. The better adhesion between matrix and fibers decreases the velocity of the diffusing molecules. Another factor is that stronger adhesion results in tighter packing within the epoxy–fiber

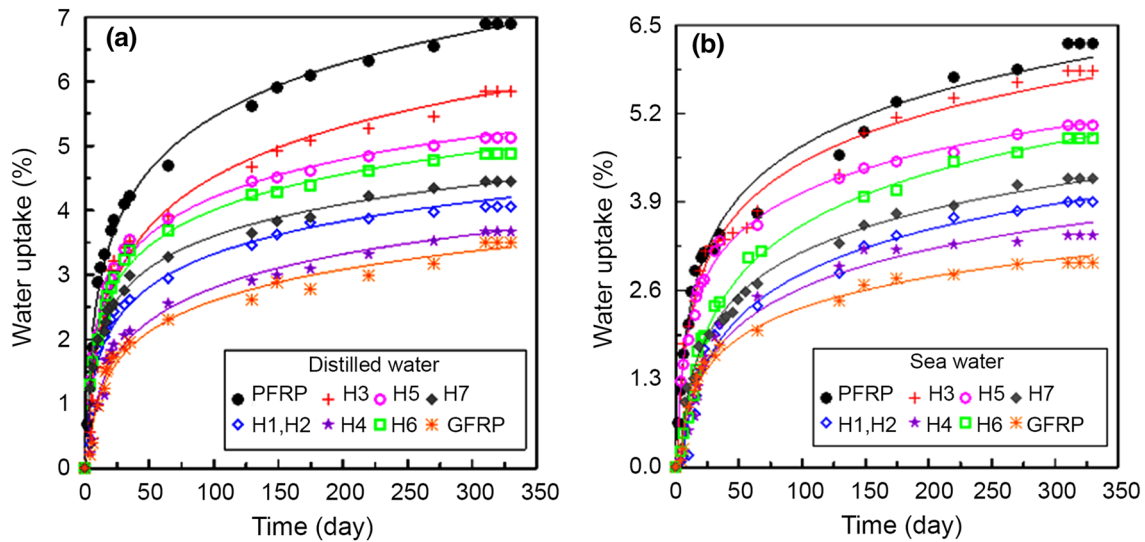


Fig. 3 Water uptake of G-P fibers reinforced epoxy composites: **a** distilled water and **b** sea water

network due to which, the distance traveled by the diffusing water molecules between two consecutive collisions would drop (mean free path) and consequently results in lower water uptake [34].

Uptake of distilled water is slightly higher than that of sea water for all studied composites. Salt-water sorption is slightly different from that of distilled water. This is due to the presence of ions in salt water [19]. This result agrees with Davies et al. [53] who pointed out that distilled water aging differs significantly from sea water aging, particularly in terms of weight gain.

## Impact strength

The impact strength of fiber-reinforced composites is affected by many factors such as the fiber and matrix types, interface properties, layering pattern, specimens' geometry and test conditions [6, 54]. The impact strength

measurement is also very sensitive toward imperfections of the samples, such as voids, bubbles, or any impurities or inclusions [55]. The impact failure of a composite takes many forms like matrix fracture; fiber/matrix debonding and fiber pull out. Even though, fiber pull out is found to be an important energy dissipation mechanism in fiber-reinforced composites [39].

Figure 4 shows that edge-wise and flat-wise impact strengths for PFRP composite are about 2.92 and 2.75 times those of GFRP one. The lowest impact strength values were observed for GFRP composite having high tensile strength and modulus (as obtained by Attia et al. [30]). The fiber/matrix adhesion to a great extent determines the strength of composites. An improved interaction can lead to perfect bonding and thus the failure of the composites can occur at relatively low impact [34]. Ray et al. [56] observed that in composites having weak interfacial bonding the crack propagates along the fiber/matrix interface causing debonding

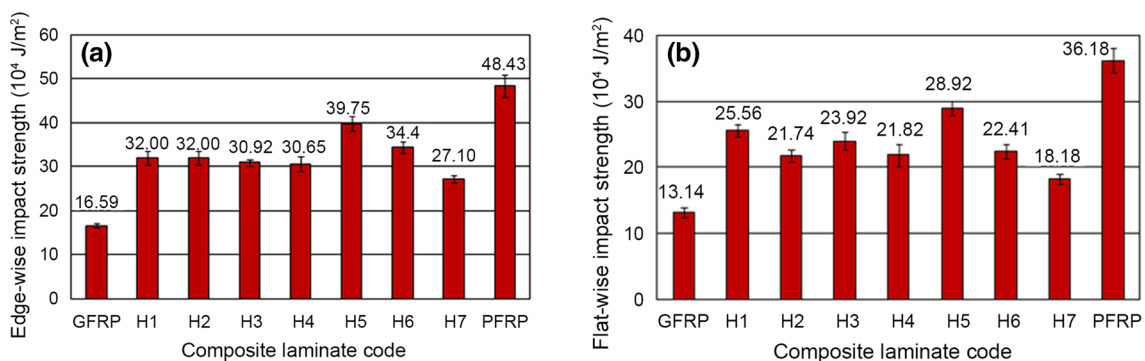


Fig. 4 Impact strength of G-P fibers reinforced epoxy composites: **a** edge-wise and **b** flat-wise



which leads to a significant increase in energy absorbing capacity of the composites. As a result, large new surfaces will be produced and the frictional work resulting from differential displacement between the matrix and fibers will increase the impact resistance of the composites.

The impact strength can be interpreted by the ability of two kinds of composites to store the impact energy in the fibers. Such energy matches the area under the tensile test curve of the fibers which is affected by elastic modulus and strain-at-failure point. The higher failure strain of P-fiber compared to G-fiber, as deduced by Attia et al. [30], means that P-fiber can absorb more energy than G-one and thus increases the impact resistance of the composite. The applied load is transferred to fibers by shear force and it exceeds the fiber/matrix interfacial bond strength and debonding occurs. Frictional losses as P-fiber is pulled out of the matrix are a major contributor to the observed toughness of PFRP composite. This result agrees with that obtained by Joseph et al. [39].

It was also noted that P–G hybrids exhibit better edge-wise and flat-wise impact strengths than those of GFRP composite. The addition of G-fiber to P-fiber restricts the deformation of P-fiber and decreases impact energy of the hybrid composites, compared to that of PFRP, through the reduction of displacement at break [57].

For inter-intrally hybrid composites, the plies stacking sequence has almost no effect on edge-wise impact strength values, whilst it has a noticeable effect on flat-wise values. Flat-wise impact response of hybrid composites appears to be dominated by the front layer [58]. Flat-wise impact strength of H1 (where P-fiber is at the impacted face) is about 1.18 times that of composite with the opposite arrangement, i.e. H2. This happens by the fact that the flexible layer at the impacted surface experiences larger deformation in composite laminates [57]. This result agrees with Park et al. [59]. Both edge-wise and flat-wise impact strengths increase when P/G fiber ratio increases.

Hybrid configuration has a noticeable effect on the impact strength values. For hybrid composites having the same P/G fiber ratio, edge-wise impact data clearly shows that intraply hybrid composite gives higher impact strength value when compared to those of inter-intrally hybrids. This is probably due to the higher efficiency in hindering crack propagation in the case of G and P fibers intimately mixed in the same layer with respect to the case in which they are located in separated plies [60].

## Morphological analysis

The interfacial bonding strength between the fiber and matrix has high influence on the impact response of the fabricated composites [9]. Failure mechanism such as fiber–matrix debonding and fiber pull out are due to the impact energy dissipation. When the pendulum strikes

the specimen, the pendulum first contacts the fiber and forces the fiber bundles to bend. Consequently, fiber pull-out, fiber breakage and fiber–matrix debonding can be observed [61]. The fractured flat-wise impact coupons exhibit delamination at the layers interface. Delamination is localized around the impacted region. The fractured notched coupons are not divided into two parts at the notches. Generally, edge-wise impact induces an opening mode force at the notch, resulting in tension failure. However, layers around the notch are delaminated and expanded and buckling occurs at the specimen back surface. Moreover fiber breakage is observed at tension side. The failure of the composite is mainly due to G-fiber breakage, P-fiber pull-out and matrix cracking [37]. Fiber pull-out is found to be the most important energy dissipation mechanism in fiber reinforced composites [39].

Figure 5 shows SEM for G–P fibers reinforced epoxy composite specimens, failed under Izod impact testing. Matrix dislocation, fiber–matrix debonding, G-fiber fracture, P-fiber pull-out, delamination and surface cracks are evident in Fig. 5a, b. The high impact strength shown by PFRP composite can be attributed to the extra energy dissipation mechanism due to plastic deformation and fiber pull-out as shown in Fig. 5. For GFRP, the fiber breakage is more likely than the plastic deformation as shown in Fig. 5b. Figure 5c shows that epoxy matrix is penetrated into G-fiber surface. It is clear from Fig. 5c that G-fibers adhere well to the matrix and undergo breaking and delamination during fracture, while Fig. 5d shows the poor interaction between P-fiber and matrix. So P-fibers are pulled out from the matrix during the impact failure. This result agrees with that obtained by Joseph et al. [39].

## Hybrid effect

The expected impact strength was calculated using the RoM which was defined simply for the impact strength as a linear relation against  $V_{ip}$ . Concretely, the straight line between the impact strength of GFRP and that of PFRP describes the RoM. A negative hybrid effect governs the impact strength of G–P hybrids as declared in Fig. 6. A positive hybrid effect was observed for edge-wise impact strengths of H5 and H6 as shown in Fig. 6a and for flat-wise impact strengths of H1 and H5 as shown in Fig. 6b. This may be due to the synergistic effect in the absorbed energy. This result agrees with that obtained by Marom et al. [62]. There are different parameters that might control the hybrid effect such as the fibers amounts, the types of fibers, relative moduli and strengths of the fibers, the nature of the fiber–matrix interface, and the arrangement of the fibers within the composite as reported by Selmy et al. [40].

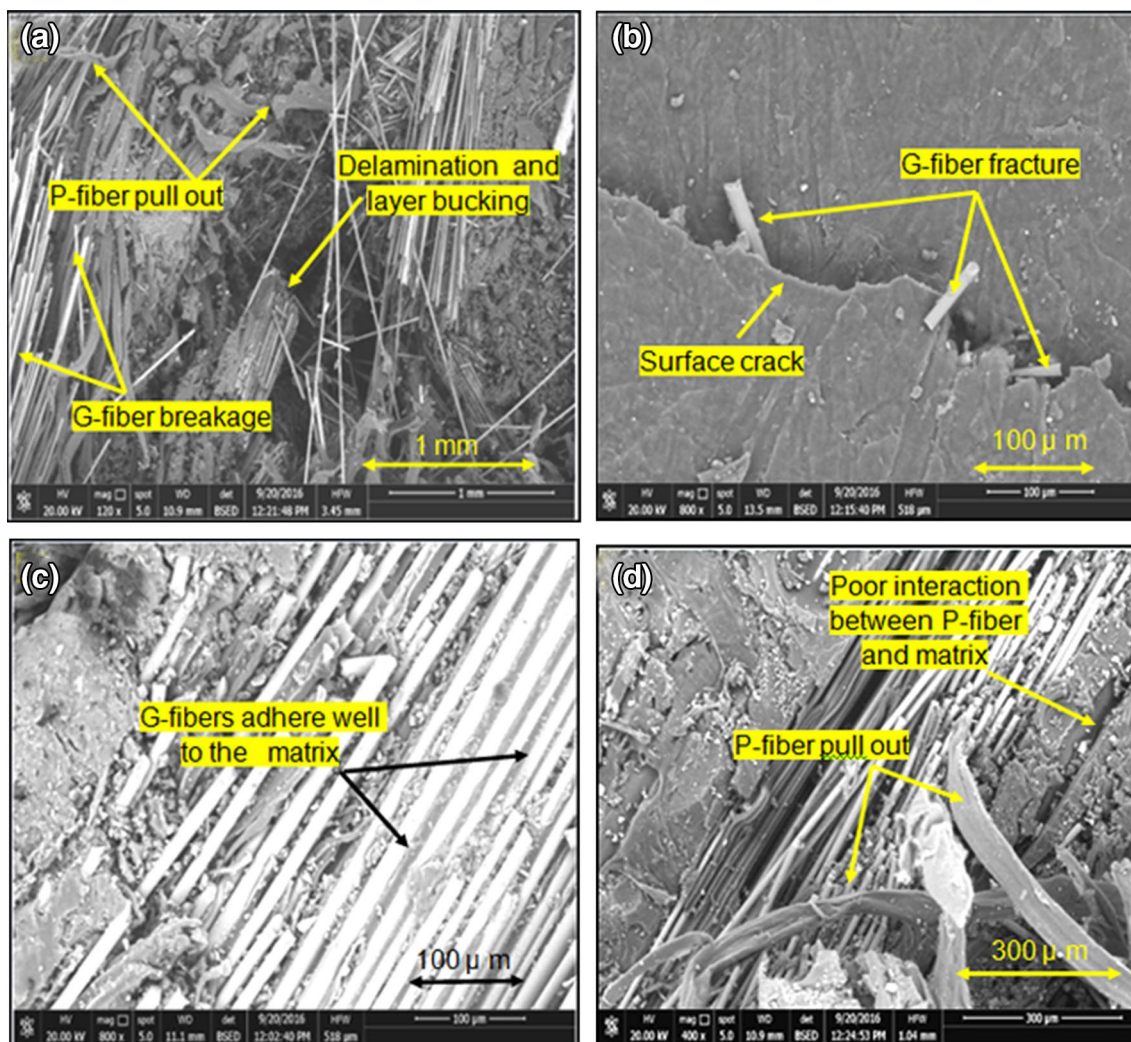


**Fig. 5** SEM for G–P fibers reinforced epoxy composite specimens failed under impact loading: **a** P-fiber pullout and delamination, **b** G-fiber fracture and surface crack, **c** good adhesion between G-fiber and matrix and **d** poor interaction between P-fiber and matrix

### Specific impact strength

Specific edge-wise and flat-wise impact strengths for G–P fibers/epoxy composites were calculated with respect to their densities and listed in Table 2. Specific edge-wise and flat-wise impact strengths of PFRP composite are about 4.43 and 4.18 times those of GFRP composite. This is due to the lower density of P-fiber compared to that of G-fiber. Both specific edge-wise and flat-wise impact strengths of G–P reinforced composites increase when P/G fiber ratio increases. For the studied inter-intraply hybrid composites, the highest specific edge-wise and flat-wise impact strengths were observed for H3 and H1, respectively.

### Strength-to-cost ratio

The cost ratios for the fabricated composites were calculated, as the impact strength is divided by the specimen cost, and compared as shown in Table 2. It is clear that the hybridization of G-fiber reinforced composites with P-fiber improves the cost ratio. From the stand point of cost, PFRP followed by H5 composites are the best choice for structures under impact loadings.

### Statistical analysis

The shape ( $\alpha$ ) and scale ( $\beta$ ) parameters of two Weibull distribution function for G–P reinforced epoxy composites were

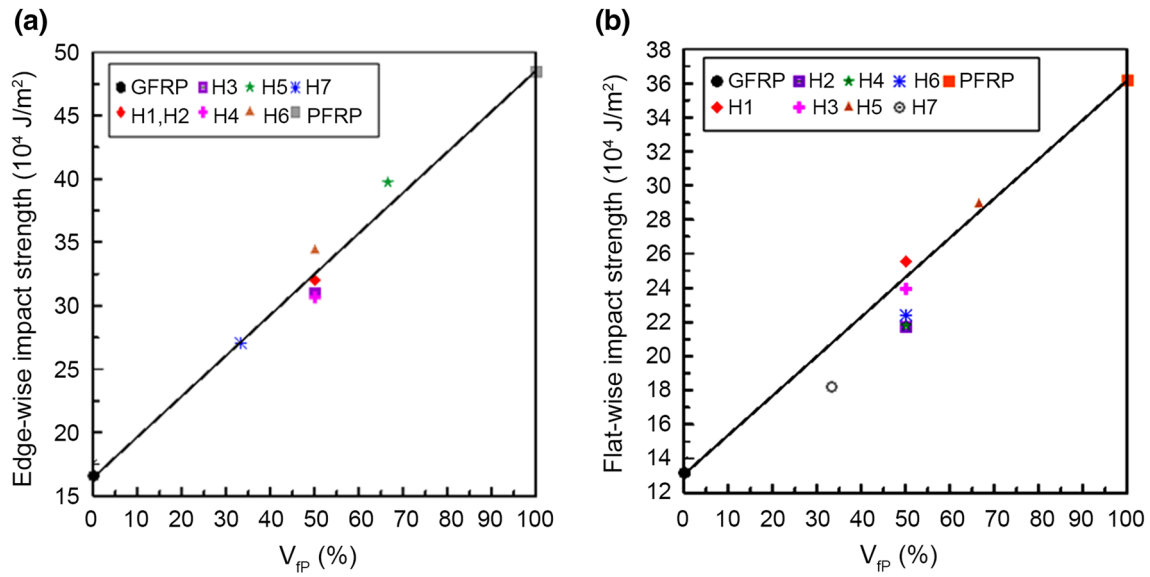


Fig. 6 Hybrid effect on the impact strength of G–P fibers reinforced epoxy composites: **a** edge-wise and **b** flat-wise

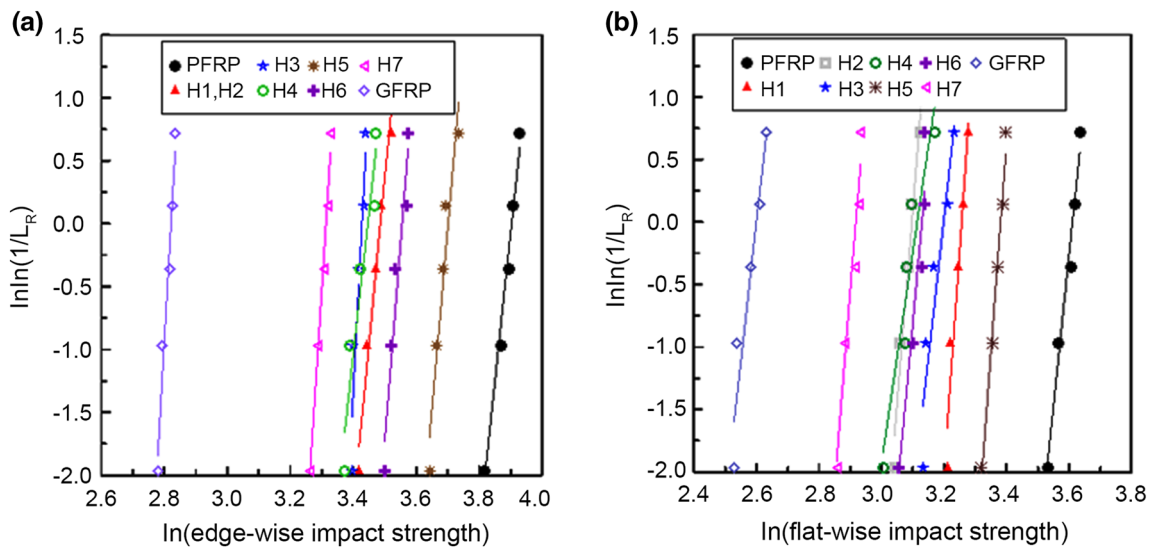


Fig. 7 Graphical analysis of impact strength data for G–P fibers reinforced epoxy composites: **a** edge-wise and **b** flat-wise

calculated graphically as shown in Fig. 7. Mean ( $M$ ), standard deviation ( $SD$ ) and coefficient of variation ( $CV$ ) of impact test results were calculated and listed in Table 3. It is clear from Table 3 that  $CV$  values range from 2.63 to 7.33%. Figure 8 shows the reliability curves of impact strength for the fabricated composite types. These graphs can be used by the design and development engineers.

### Conclusion

The main aim of this study was to create a new composite system having high-impact performance, light weight, reduced water absorption and cost-effective. To attain this aim, P–G/epoxy hybrid composites have been developed

Table 3 Statistical analysis of impact strength data for G-P fibers reinforced epoxy hybrid composites

Laminate code	Sample no.	Impact strength ( $10^4 \text{ J/m}^2$ )		Laminate code	Sample no.	Impact strength ( $10^4 \text{ J/m}^2$ )		Laminate code	Sample no.	Impact strength ( $10^4 \text{ J/m}^2$ )	
		Edge-wise	Flat-wise			Edge-wise	Flat-wise			Edge-wise	Flat-wise
PFRP	1	45.37	34.15	H3	1	29.92	22.94	H6	1	33.12	22.89
	2	47.89	36.78		2	29.85	23.67		2	33.87	21.19
	3	49.12	37.87		3	31.18	23.18		3	35.69	23.08
	4	49.67	37.32		4	30.56	24.79		4	34.19	22.17
	5	50.85	35.33		5	31.04	25.37		5	35.53	23.02
$\alpha$		23.57	24.15	$\alpha$		48.48	22.38	$\alpha$		31.15	27.20
$\beta$		49.56	37.01	$\beta$		31.28	24.50	$\beta$		35.01	22.87
$M$		48.43	36.18	$M$		30.92	23.92	$M$		34.40	22.41
SD		2.55	1.87	SD		0.81	1.33	SD		1.39	1.04
CV (%)		5.26	5.16	CV (%)		2.63	5.56	CV (%)		4.04	4.63
H1	1	30.54	25.02	H4	1	29.17	20.18	H7	1	27.29	18.44
	2	32.17	24.78		2	29.69	21.67		2	26.76	18.66
	3	33.78	26.05		3	30.62	22.09		3	27.89	18.78
	4	31.29	25.66		4	31.99	21.78		4	26.13	17.83
	5	32.67	26.54		5	32.23	23.78		5	27.68	17.39
$\alpha$		26.27	35.68	$\alpha$		22.59	16.82	$\alpha$		38.92	31.03
$\beta$		32.67	25.96	$\beta$		31.39	22.52	$\beta$		27.49	18.50
$M$		32.00	25.56	$M$		30.65	21.82	$M$		27.10	18.18
SD		1.52	0.89	SD		1.69	1.60	SD		0.87	0.73
CV (%)		4.74	3.46	CV (%)		5.51	7.33	CV (%)		3.21	4.02
H2	1	30.54	20.94	H5	1	38.19	29.13	GFRP	1	16.12	13.23
	2	32.17	22.07		2	39.88	28.65		2	16.89	12.53
	3	33.78	21.32		3	40.23	29.89		3	17.02	13.89
	4	31.29	22.79		4	39.04	27.66		4	16.34	12.65
	5	32.67	21.83		5	41.91	29.62		5	16.73	13.60
$\alpha$		26.27	31.09	$\alpha$		28.72	33.54	$\alpha$		44.53	22.30
$\beta$		32.67	22.13	$\beta$		40.52	29.41	$\beta$		16.80	13.46
$M$		32.00	21.74	$M$		39.75	28.92	$M$		16.59	13.14
SD		1.52	0.87	SD		1.73	1.08	SD		0.49	0.74
CV (%)		4.74	4.02	CV (%)		4.36	3.74	CV (%)		2.92	5.6

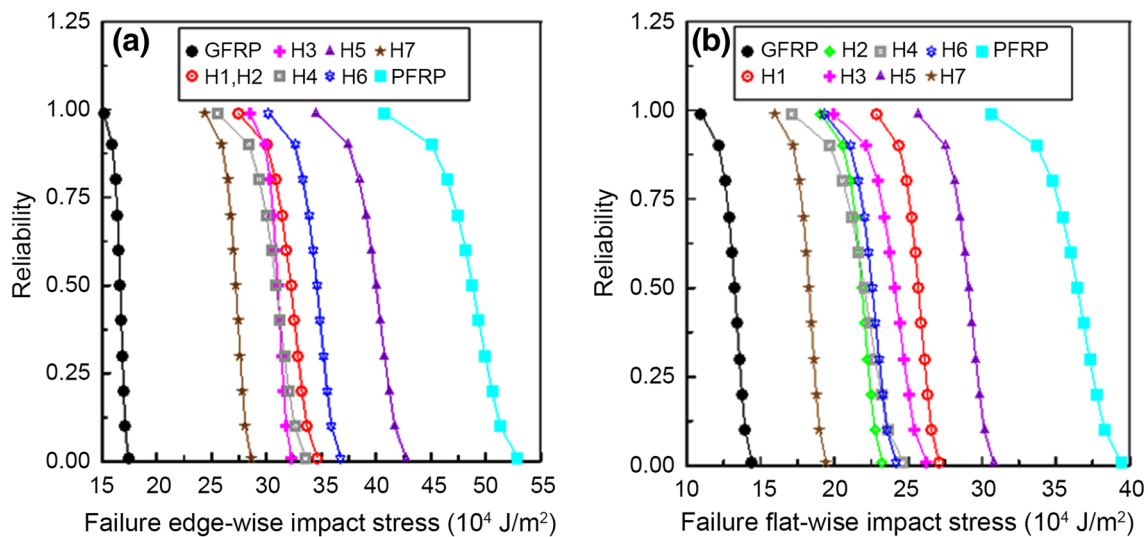


**Fig. 8** Reliability curves for G–P fibers reinforced epoxy composites: **a** edge-wise and **b** flat-wise

as a function of plies stacking sequence, hybrid configuration, P/G fiber ratio and test direction (edge-wise or flat-wise). Based on the obtained results, the following conclusions are reached:

- Hybridizing G-fiber reinforced composite with P-fiber, decreases the composite density, due to the low density of the P-fiber, but increases the void content, due to the incompatibility between the epoxy resin and P-fiber leading to incomplete wetting of the fibers by the matrix. As P/G fibers ratio increases, the water uptake increases due to the hydrophilic nature of P-fiber and the capillary action when fiber ends are exposed to water.
- The hybrid composite, with G-fiber at the periphery and P-fiber at the core, has lower void content because P-fiber in the specimen core is tightly packed by G-fiber and lower water uptake because G-fiber acts as a barrier to the P-fiber, thus preventing the direct contact between the P-fiber and water compared with the opposite arrangement. Distilled water uptake is slightly higher than sea water uptake for all studied composites due to the presence of ions in salt water. From the stand point of cost, PFRP followed by H5 composites are the best for structures used under impact loadings.
- The plies stacking sequence has almost no effect on edge-wise impact strength values, whilst it has a noticeable effect on flat-wise ones. When P-layers are at the impacted face, the composite exhibits higher impact strength. This happens by the fact that the flexible layer at the impacted surface experiences larger deformation in composite laminates. Both edge-wise and flat-wise impact strengths increase when P/G fiber ratio increases.

That is because P-fiber is more ductile and can absorb more energy.

- Edge-wise impact data clearly showed that intraply hybrid composite displayed higher impact strength value when compared to those of inter-intraply hybrids. This is due to the higher efficiency in hindering crack propagation in the case of G and P fibers intimately mixed in the same layer with respect to the case in which they are located in separated plies.
- A negative hybrid effect governs the impact strength of G–P hybrids except for H5 and H6 for edge-wise impact strength and H1 and H5 for flat-wise impact strength. This may be due to the synergistic effect in the absorbed energy.
- Two-parameter Weibull distribution was used to analyze the impact results. The reliability curves have been extracted to be used by design engineers.
- Briefly, PFRP composites have better impact strength and low cost whilst the water uptake resistance of GFRP is better. Therefore, combining the P-fiber and G-fiber through the formation of hybrid composite will make the obtained hybrid systems having the privileges of P-fiber and G-fiber into a single hybrid system.

## References

1. Wang J, Zhao J, Liu T, He Z, Li K, Yang W (2015) Crash analysis of composite energy-absorbing cylindrical impact attenuator. *J Reinf Plast Compos* 34:2006–2017
2. Sarasini F, Tirill J, Valente M, Valente T, Cioffi S, Iannace S, Sorrentino L (2013) Effect of basalt fiber hybridization on the impact

- behavior under low impact velocity of glass/basalt woven fabric/epoxy resin composites. *Compos Part A* 47:109–123
3. John MJ, Varughese KT, Thomas S (2008) Green composites from natural fibers and natural rubber: effect of fiber ratio on mechanical and swelling characteristics. *J Nat Fiber* 5:47–60
  4. Kalaprasad G, Joseph K, Thomas S (1997) Influence of short glass fiber addition on the mechanical properties of sisal reinforced low density polyethylene composites. *J Compos Mater* 31:509–527
  5. De Rosa IM, Santulli C, Sarasini F, Valente M (2009) Post-impact damage characterization of hybrid configurations of jute/glass polyester laminates using acoustic emission and IR thermography. *Compos Sci Technol* 66:1142–1150
  6. Acikbas G, Ozcan S, Acikbas NC (2017) Production and characterization of a hybrid polymer matrix composite. *Polym Compos* <https://doi.org/10.1002/pc.24471> (In press)
  7. Idicula M, Malhotra SK, Joseph K, Thomas S (2005) Effect of layering pattern on dynamic mechanical properties of randomly oriented short banana/sisal hybrid fiber–reinforced polyester composites. *J Appl Polym Sci* 97:2168–2174
  8. Pothan LA, George J, Oommen Z, Thomas S (1999) Polyester composites of short banana fibers and glass fibers. Tensile and impact properties. *Polimery Nr* 44:750–757
  9. Pothan LA, George CN, John MJ (2010) Dynamic mechanical and dielectric behavior of banana–glass hybrid fiber reinforced polyester composites. *J Reinf Plast Compos* 29:1131–1145
  10. Pincheira G, Canales C, Medina C, Fernandez E, Flores P (2018) Influence of aramid fibers on the mechanical behavior of a hybrid carbon–aramid-reinforced epoxy composite. *Proc Inst Mech Eng Part L J Mater Design Appl* 232:58–66
  11. Davoodi MM, Sapuan SM, Ahmad D, Aidy A, Khalina A, Jonoobi M (2011) Concept selection of car bumper beam with developed hybrid bio-composite material. *Mater Des* 32:4857–4865
  12. Boopalan M, Niranjanaa M, Umopathy MJ (2013) Study on the mechanical properties and thermal properties of jute and banana fiber reinforced epoxy hybrid composites. *Compos Part B Eng* 51:54–57
  13. Dehkordi MT, Nosratty H, Shokrieh MM, Minak G, Ghelli D (2010) Low velocity impact properties of intra-ply hybrid composites based on basalt and nylon woven fabrics. *Mater Des* 31:3835–3844
  14. Wang X (2008) Low velocity impact properties of 3D woven basalt/aramid hybrid composites. *Compos Sci Technol* 68:444–450
  15. Panthapulakkal S, Sain M (2007) Injection-molded short hemp fiber/glass fiber reinforced polypropylene hybrid composites-mechanical, water absorption and thermal properties. *J Appl Polym Sci* 103:2432–2441
  16. Venkateshwaran N, Elaya Perumal A, Alavudeen A, Thiruchitrambalam M (2011) Mechanical and water absorption behaviour of banana/sisal reinforced hybrid composites. *Mater Des* 32:4017–4021
  17. Visco AM, Campo N, Cianciafara P (2011) Comparison of seawater absorption properties of thermoset resins based composites. *Compos Part A* 42:123–130
  18. Dhakal HN, Zhang ZY, Richardson MAW (2007) Effect of water absorption on the mechanical properties of hemp fibre reinforced unsaturated polyester composites. *Compos Sci Technol* 67:1674–1683
  19. Sreekala MS, George J, Kumaran MG, Thomas S (2001) Water-sorption kinetics in oil palm fibers. *J Polym Sci Part B Polym Phys* 39:1215–1223
  20. Koradiya SB, Patel JP, Parsania PH (2010) The preparation and physicochemical study of glass, jute and hybrid glass–jute bisphenol-C-based epoxy resin composites. *Polym-Plast Technol Eng* 49:1445–1449
  21. Priya SP, Rai SK (2006) Mechanical performance of biofiber/glass reinforced epoxy hybrid composites. *J Indust Text* 35:217–226
  22. Jarukumjorn K, Suppakarn N (2009) Effect of glass fiber hybridization on properties of sisal fiber-polypropylene composites. *Compos Part B-Eng* 40:623–627
  23. Joseph S, Sreekala MS, Koshy P, Thomas S (2008) Mechanical properties and water sorption behavior of phenol-formaldehyde hybrid composites reinforced with banana fiber and glass fiber. *J Appl Polym Sci* 109:1439–1446
  24. Burrow MF, Thomas D, Swain MV, Tyas MJ (2004) Analysis of tensile bond strengths using Weibull statistics. *Biomaterials* 25:5031–5035
  25. Selmy AI, Abd El-baky MA, Azab NA (2013) Experimental study on flexural fatigue behavior of glass fibers/epoxy hybrid composites with statistical analysis. *J Reinf Plast Compos* 32:1821–1834
  26. Gorjan L, Ambro M (2012) Bend strength of alumina ceramics: a comparison of Weibull statistics with other statistics based on very large experimental data set. *J Eur Ceram Soc* 32:1221–1227
  27. Mottram JT (1994) Compression strength of pultruded sheet material. *J Mater Civil Eng* 6:185–200
  28. Selmy AI, Azab NA, Abd El-baky MA (2014) Statistical analysis of monotonic mechanical properties for unidirectional glass fiber (U)/random glass fiber (R)/epoxy hybrid and non-hybrid polymeric composites. *J Compos Mater* 48:455–469
  29. Wu D, Zhou J, Li Y (2006) Methods for estimating Weibull parameters for brittle materials. *J Mater Sci* 41:5630–5638
  30. Attia MA, Abd El-baky MA, Alshorbagy AE (2017) Mechanical performance of intraply and inter-intraply hybrid composites based on e-glass and polypropylene unidirectional fibers. *J Compos Mater* 51:381–394
  31. Faidh-Allah MH, Ismail SA (2018) Optimization of cutting parameters on delamination of drilling glass-polyester composites. *J Eng* 24:34–45
  32. ASTM D570-98 (Reapproved 2005), Standard test method for water absorption of plastics
  33. Sreekala MS, Kumaran MG, Joseph R, Thomas S (2001) Stress-relaxation behaviour in composites based on short oil-palm fibres and phenol formaldehyde resin. *Compos Sci Technol* 61:1175–1188
  34. Sreekumar PA, Thomas SP, Saiter JM, Joseph K, Unnikrishnan G, Thomas S (2009) Effect of fiber surface modification on the mechanical and water absorption characteristics of sisal/polyester composites fabricated by resin transfer molding. *Compos A* 40:1777–1784
  35. Sari PS, Spatenka P, Jenikova Z, Grohens Y, Thomas S (2015) New type of thermoplastic biocomposites: nature of the interface on the ultimate properties and water absorption. *RSC Adv* 5:97536–97546
  36. Pothan LA, Thomas S, Neelakantan NR (1997) Short banana fiber reinforced polyester composites: mechanical, failure and aging characteristics. *J Reinf Plast Compos* 16:744–765
  37. Sreekala MS, Thomas S, Neelakantan NR (2011) Utilization of short oil palm empty fruit bunch fiber (OPEFB) as reinforcement in phenol-formaldehyde resins: studies on mechanical properties. *J Polym Eng* 16:265–294
  38. ISO (2000) 180:2000 (E) Plastics-determination of Izod impact strength, European Standards, Int Org for Standardization: Switzerland, 3rd edn
  39. Joseph S, Sreekala MS, Oommen Z, Koshy P, Thomas S (2002) A comparison of the mechanical properties of phenol formaldehyde composites reinforced with banana fibres and glass fibres. *Compos Sci Technol* 62:1857–1868
  40. Selmy AI, Abd El-baky MA, Hegazy DA (2018) Mechanical properties of inter-ply hybrid composites reinforced with glass

- and polyamide fibers. *J Thermoplast Compos Mater*. <https://doi.org/10.1177/0892705717751022>
41. Attia MA, Abd El-Baky MA, Hassan MA, Sebaey TA, Mahdi E (2017) Crashworthiness characteristics of carbon–jute–glass reinforced epoxy composite circular tubes. *Polym Compos*. <https://doi.org/10.1002/pc.24597>
  42. Acikbas NC, Acikbas G (2017) Epoxy matrix composites containing urea formaldehyde waste particulate filler. *Waste Biomass Valor* 8:669–678
  43. Abd El-baky MA (2017) Evaluation of mechanical properties of jute/glass/carbon fibers reinforced hybrid composites. *Fiber Polym* 18:2417–2432
  44. ASTM D 2734 (2009) Standard test methods for void content of reinforced plastics
  45. Abdallah MH, Abdin EM, Selmy AI, Khashaba UA (1996) Reliability analysis of GFRP pultruded composite rods. *Int J Qual Reliab Manage* 13:88–98
  46. Khashaba UA (2003) Fatigue and reliability analysis of unidirectional GFRP composites under rotating bending loads. *J Compos Mater* 37:317–331
  47. Selmy AI, Abd El-baky MA, Ghazy MR, Kamel M (2017) Flexural fatigue performance of glass fiber/epoxy step-wise functionally and non-functionally graded composites of different structures. *Int Polym Proc* 32:298–307
  48. Sakin R, Ay I (2008) Statistical analysis of bending fatigue life data using Weibull distribution in glass-fiber reinforced polyester composites. *Mater Des* 29:1170–1181
  49. Selmy AI, Abd El-baky MA, Ghazy MR, Kamel M (2015) In-plane shear characteristics of unidirectional glass fiber/epoxy functionally graded (FG) and nonfunctionally graded (NFG) composite laminates with statistical analysis. *J Compos Mater* 49:3347–3358
  50. Abd El-baky MA, Attia MA, Kamel M (2018) Flexural fatigue and failure probability analysis of polypropylene-glass hybrid fibres reinforced epoxy composite laminates. *Plast Rubber Compos* 47:47–64
  51. Dirikoglu MH, Aktas A (2002) Statistical analysis of fracture strength of composite materials using Weibull distribution. *Turk J Eng Environ Sci* 26:45–48
  52. Zhou G, Davies GAO (1995) Characterization of thick glass woven-roving/polyester laminates: flexure and statistical considerations. *Composites* 26:587–596
  53. Davies P, Mazeas M, Casari P (2001) Sea water aging of glass reinforced composites. Shear behaviour and damage modelling. *J Compos Mater* 35:1343–1372
  54. Alavudeen A, Rajini N, Karthikeyan S, Thiruchitrambalam M, Venkateshware N (2015) Mechanical properties of banana/kenaf fiber-reinforced hybrid polyester composites: effect of woven fabric and random orientation. *Mater Des* 66:246–257
  55. Muhammad YH, Ahmad S, Abu Bakar MA, Mamun AA, Heim HP (2015) Mechanical properties of hybrid glass/kenaf fibre-reinforced epoxy composite with matrix modification using liquid epoxidised natural rubber. *J Reinf Plast Compos* 34:896–906
  56. Ray D, Sarkar BK, Rana AK, Bose NR (2001) The mechanical properties of vinylester resin matrix composites reinforced with alkali-treated jute fibers. *Compos Part A Appl Sci Manuf* 32:119–127
  57. Rahmanian S, Thean KS, Suraya AR, Shazed MA, Salleh MAM, Yusoff HM (2013) Carbon and glass hierarchical fibers: influence of carbon nanotubes on tensile, flexural and impact properties of short fiber reinforced composites. *Mater Des* 43:10–16
  58. Fragassa C, Pavlovic A, Santulli C (2018) Mechanical and impact characterization of flax and basalt fibre vinylester composites and their hybrids. *Compos Part B: Eng* 137:247–259
  59. Park R, Jang J (2001) Impact behavior of aramid fiber/glass fiber hybrid composites: the effect of stacking sequence. *Polym Compos* 22:80–89
  60. Pegoretti A, Fabbri E, Migliaresi C, Pilati F (2004) Intraply and interply hybrid composites based on E-glass and poly(vinyl alcohol) woven fabrics: tensile and impact properties. *Polym Int* 53:1290–1297
  61. Kim JK, Sham ML (2000) Impact and delamination failure of woven-fabric composites. *Compos Sci Technol* 60:745–761
  62. Marom G, Fischer S, Tuler FR, Wagner HD (1978) Hybrid effects in composites: conditions for positive or negative effects versus rule of mixtures behavior. *J Mater Sci* 13:1419–1426